Journal of Materials Chemistry A

PAPER

Check for updates

Cite this: J. Mater. Chem. A, 2017, 5, 21947

Redox synthesis and high catalytic efficiency of transition-metal nanoparticle–graphene oxide nanocomposites†

Changlong Wang,[ab] Roberto Ciganda,[a] Luis Yate,[c] Jimena Tuninetti,[cd] Victoria Shalabaeva,[b] Lionel Salmon,[b] Sergio Moya,[c] Jaime Ruiz[a] and Didier Astruc*[a]

Received 15th July 2017
Accepted 2nd October 2017

DOI: 10.1039/c7ta06182j

rsc.li/materials-a

Although nanocatalysis is a promising area, increased efficiency and greenness are actively sought. Here we report the principle of the syntheses of graphene oxide (GO)-supported metal nanocatalysts (MNPs) for a variety of transition metals including both noble metals and biometal using either exergonic or endergonic redox reactions between GO and the transition metal salts. These new nanocatalysts are highly efficient in water at ambient temperature for 4-nitrophenol reduction (the test reaction), Sonogashira coupling, azide–alkyne 1,3-cycloaddition (click reaction) and dihydrogen production upon hydrolysis of ammonia–borane and recyclable.

1. Introduction

Nanocatalysis is a very promising area,[1–13] because high performance nanoparticles (NPs) may be efficiently designed in the absence of ligands that are often toxic, expensive, sensitive and/or of time-consuming synthesis. A variety of organic and inorganic nanocatalyst stabilizers have also been reported, but they usually damage the catalytic activity and may be difficult to remove.[14–22] Among heterogeneous catalyst supports, carbon materials have proven remarkable because of possible synergetic catalytic activation.[23–39] Carbon-supported NPs are usually obtained by metal cation reduction using various reductants, but catalysis may be marred by the reactant residue on the NP surface. Clean direct metal cation reduction by carbon materials has rarely been reported, however. Recently Dai's group utilized single-walled carbon nanotubes (SWNT) sidewall as reductant and stabilizer.[30] Redox-mediated nanocatalyst synthesis has also been demonstrated by Chen's group and Tang's group who utilized graphene oxide (GO) and reduced GO as redox mediator to provide efficient noble metal nanocatalysts with Pd and Au respectively.[31,32]

Here we report the general redox synthesis of green graphene-oxide-supported transition metal nanoparticle catalysts as a clean and most useful synthetic method of NP/GO catalyst avoiding the use of external reductant. This method applies here from noble metals for which the electron transfer from GO is exergonic, thus favorable, to first-raw biometals for which this redox process is endergonic but nevertheless accomplished owing to the fast follow-up NP formation. This concept is also extended to bimetallic NP–graphene oxide composites that include a noble metal and a biometal. It is very efficiently applied here to a variety of reactions in water at room temperature (rt) with remarkably low amounts of catalytic metals including 4-nitrophenol reduction (a reaction used as a test to optimize catalyst preparations), Sonogashira coupling, azide–alkyne 1,3-cycloaddition (click reaction) and dihydrogen production upon hydrolysis of ammonia–borane.

2. Experimental section

2.1. General data

All solvents and chemicals were used as purchased. Prior to the synthesis, all the flask were washed with a solution of aqua regia ($HCl/HNO_3 = 3:1$ v/v) to remove any traces of metal residue. Milli-Q water (18.2 MΩ) was used for all the preparations. NMR spectra were recorded at 25 °C with a Bruker AC 300, or 400 (300 or 400 MHz). All the chemical shifts are reported in parts per million (δ, ppm) with reference to Me_4Si for the ^1H NMR spectra. UV-vis. absorption spectra were measured with a Perkin-Elmer Lambda 19 UV-vis. spectrometer. The Rh content was quantified by inductively coupled plasma atomic emission

[a]ISM, UMR CNRS No 5255, Univ. Bordeaux, 33405 Talence Cedex, France. E-mail: didier.astruc@u-bordeaux.fr

[b]Laboratoire de Chimie de Coordination, UPR CNRS 8241, 31077 Toulouse Cedex, France

[c]CIC biomaGUNE, Unidad Biosuperficies, Paseo Miramon No 182, Edif "C", 20009 Donostia-San Sebastian, Spain

[d]Instituto de Investigaciones Fisicoquímicas Teóricas y Aplicadas (INIFTA), Universidad Nacional de La Plata – CONICET, Diagonal 113 y 64, 1900 La Plata, Argentina

† Electronic supplementary information (ESI) available: Synthesis and characterization of the nanocatalysts. ^1H NMR spectra of the products. UV-vis. spectra monitoring nitrophenol reduction, hydrolysis of AB reactions, click reactions and Sonogashira reactions. See DOI: 10.1039/c7ta06182j

This journal is © The Royal Society of Chemistry 2017

spectroscopy (ICP-AES) using a Thermo Scientific iCAP 6300 DUO spectrometer with a 3-channel, 12-roller pump and a 27.12 MHz solid state RF plasma generator. Raman spectroscopy: Raman spectra were collected between 350 and 80 K using a LabRAM-HR (Jobin-Yvon) Raman micro-spectrometer and a Linkam THMS-600 cryostage. The 632.8 nm line of a He–Ne laser was used as the excitation source and a spectral resolution of approximately 3 cm^{-1} was obtained. Transmission Electron Microscopy (TEM) and high-resolution Electron Microscopy (HRTEM) images were recorded by A TEM JEOL JEM 1400 (120 kV) and a high-resolution TEM JEOL JEM 2100F (200 kV) that was equipped with a PGT X-ray analyzer were used for size and composition analysis. Size was calculated based on at least 100 NPs. X-ray photoelectron spectra (XPS): System: SPECS SAGE HR, X-ray source: Mg Kα non-monochromatic, operated at 12.5 kV and 250 W. Take off angle 90°, at ~10–8 Torr. Pass energy for survey spectra 30 eV, 15 eV for narrow scans. Analysis: spectra are calibrated to CC carbon 285 eV. Analysis consisted of Shirley background subtraction. Peaks are fitted with symmetrical Gaussian–Lorentzian (GL) line shapes. Sample is dispersed on silica substrate and its solvent evaporated prior to measurement.

2.2. Synthesis of the nanocatalysts

Taking the synthesis of RhNP/GO as an example: in a typical synthesis procedure, 45 mg of GO was dispersed in 100 mL of water to obtain a yellow colored solution with ultrasonic treatment. Then, 6 mL of this GO solution was taken and injected into a Schlenk flask with continuous stirring at the given temperature in an oil bath. The temperature of the GO solution is controlled by an external thermometer. When the given temperature was reached, a 1 mL aqueous solution of metal precursors was then added dropwise. The mixture was allowed to further stir for 30 min, and the resulting catalyst was collected by centrifugation and washed with water, and then re-dispersed in water. The metal content was quantified by inductively coupled plasma atomic emission spectroscopy (ICP-AES). For instance it was found using this method that the Rh content was *ca.* 15.9 wt%. XPS was used to determine the atomic percentage, and the atomic percentage of Rh, Cu, Pd, PdCu is 1.9%, 2.1%, 2.7%, 2.2% respectively.

2.3. Catalytic activity measurements

(1) Reduction of 4-NP by $NaBH_4$ (at 20 °C): the catalytic efficiencies of the RhNPs/GO nanocatalysts were tested by the model reaction of 4-NP reduction with excess of $NaBH_4$ that is fast, simple and well controlled. Generally, 4-NP (0.05 mmol, 1 equiv.) was mixed with excess $NaBH_4$ (81 equiv.) in water under air. The color of the solution changed from light yellow to dark yellow due to the formation of the 4-NPate anion. A diluted solution containing various amounts of RhNPs/GO nanocatalysts was added to the mixture. Then, the solution quickly lost its dark yellow color with time, and the progress of the reaction was monitored by UV-vis. spectroscopy (40 s for each run).

(2) Dehydrogenation of $H_3N–BH_3$ by RhNPs/GO nanocatalyst: generally, the hydrolysis reactions of $H_3N–BH_3$ were conducted under air in water at the given experimental temperature. An aqueous solution of $H_3N–BH_3$ (42.5 mg, 1.38 mmol) was prepared in a round bottom 50 mL flask fitted with a gas outlet and a side arm sealed with a tight-fitting septum cap. The flask was connected *via* the gas outlet to a water-filled gas burette. The catalyst was then syringed through the septum, the magnetic stirring was connected and timing started. The total volume of water in all the reactions was fixed at 3 mL. Gas evolution began immediately and the amount of gas evolved was determined periodically by measuring the displacement of water in the burette. In our case, a quantitative conversion of $H_3N–BH_3$ produced 3.0 equivalents of H_2, and occupied *ca.* 100 mL at atmospheric pressure. Prior to the reactions, the volumes were measured at atmospheric pressure and corrected for water vapor pressure at room temperature.

(3) Azide–alkyne cycloaddition reactions: a glass vessel equipped with a magnetic stir bar was charged with benzyl azide (0.10 mmol) and phenylacetylene (0.105 mmol) under Ar. The catalyst was added into the vessel under Ar, and water was added in order to obtain a given volume of aqueous solution (1 mL). The reaction mixture was then stirred for 24 h at 35 °C under Ar. After the reaction, 5 mL water was added and the final product was extracted from water with CH_2Cl_2 (3 × 5 mL). The organic layer was dried over Na_2SO_4 and filtered, and the solvent was removed *in vacuo* to give the 1-benzyl-4-phenyl-1*H*-[1,2,3] triazole. Crude product was checked by ^1H NMR to calculate the conversion. In parallel, the reaction was checked using TLC. The product was then purified by silica chromatography.

(4) Sonogashira Reaction: a dry Schlenk flask equipped with a magnetic stir bar was charged with iodobenzene (0.5 mmol, 1 equiv.), alkyne (1.2 equiv.), and triethylamine (3 equiv.) under Ar. The catalyst (0.05 mol%) was then added under Ar, and water was then added in order to obtain a given volume of aqueous solution (2 mL). The mixture was allowed to stir for 24 h at room temperature. After the reaction, 3 mL water was added and the aqueous phase was extracted three times with 5 mL Et_2O. The organic phase was dried over Na_2SO_4, and the solvent was removed *in vacuo*. In parallel, the reaction was checked using TLC with petroleum ether as the eluent and ^1H NMR spectroscopy. Purification by flash chromatography was conducted with silica gel as the stationary phase and petroleum ether as the mobile phase. No yield difference when water/EtOH mixture (1 : 1, 2 mL) solvent was used.

3. Results and discussions

3.1. Characterizations

Rh NPs have not so far been generated by redox mediation with GO, but the oxidation potential of GO (0.48 V *vs.* SCE)[31] and the redox potential of Rh^{3+}/Rh (0.76 V *vs.* SCE),[33] should in principle allow an exergonic primary electron transfer between GO and Rh^{3+}. Thus the redox-mediated synthesis of GO-stabilized RhNPs should be applicable for the production of a clean Rh-based nanocatalyst as our present results demonstrate.

First, GO was synthesized from commercial graphite using the modified Hummers method,[34] and transmission electron microscopy (TEM) images showed layered and flat structures

 This journal is © The Royal Society of Chemistry 2017

(Fig. S1†), then sonication, and stirring formed a GO dispersion. Let us take the synthesis of RhNPs/GO nanocatalyst as the first example. RhNPs/GO was prepared by dropwise addition of an aqueous solution of $RhCl_3$ to the GO dispersion by syringe at 0 °C followed by further stirring for another 30 min (Experimental section and Fig. S2†). UV-vis. spectroscopy was used to monitor the reduction process with the rhodium *d–d* transition absorbance at 379 nm and 480 nm gradually decreasing with time, verifying the reduction of Rh^{3+} to Rh(0) by GO.[35] The reduction process was faster upon increasing the temperature. For instance the reduction of Rh^{3+} to Rh(0) by GO at 45 °C took only 1 min, whereas at 0 °C it required 30 min (Fig. S4†). The observed enhanced efficiency in the synthesis is attributed to an instantaneous nucleation process upon increasing the reaction temperature, resulting in reduced RhNP size (Table 1). Ostwald ripening takes place at higher temperature (>45 °C) following Rh atom nucleation, however, leading to the decrease in the number of Rh nuclei and to RhNP overgrowth.[33] Moreover after collecting by centrifugation, washing and redispersion in water, the nanocatalyst underwent a darker-to-lighter color change with increased temperatures, which is presumably related to the changes of RhNP size (Fig. S5†). Taken together, these phenomena indicate that the choice of the appropriate temperature in the synthesis optimizes the interaction between the RhNPs and the GO, a higher temperature weakening the GO anchoring ability and increasing the mobility of the Rh nuclei on the GO surface.[31–33,36–38]

Fig. 1a shows the STEM image of RhNP/GO from the synthesis at 45 °C. It is striking that the 1.8 ± 0.3 nm RhNPs are fairly monodisperse on the GO surfaces. A high-resolution TEM (HRTEM) image (Fig. 1b) of the RhNPs shows that the interplanar spacing of the particle lattice is 0.23 nm, corresponding to the (111) lattice spacing of face centered cubic Rh. X-ray photoelectron spectroscopy (XPS) was further recorded to investigate the surface nature of the RhNPs and GO. Comparison of the binding energy (B.E.) between the C 1s spectra of GO and RhNP/GO clearly shows that after the reaction the peaks associated with the C–C bonds (B.E. = 284.6 eV) become predominant (Fig. 1c), whereas the additional peak of C–O (B.E. = 286.6 eV) decreases during Rh^{3+} reduction (Fig. 1d).[31] The reducing nature of GO is due to the oxygenated functional groups attached to the hexagonal basal plane, further suggesting that these oxygenated functional groups (*e.g.* –OH, –COOH, epoxy) on the GO nanosheets play an important role of nanoparticles

Table 1 4-NP reduction catalyzed by RhNPs/GO[a]

Catalyst	Size[b] (nm)	Amount[c]	k_{app}[d] ($\times 10^{-3}$ s^{-1})
RhNP/GO-0 °C	3.6 ± 0.4	10 ppm/(1 ppm)	7.16/(3.13)
RhNP/GO-20 °C	2.6 ± 0.3	10 ppm	8.9
RhNP/GO-45 °C	1.8 ± 0.3	10 ppm/(1 ppm)	11.8/(4.29)
RhNP/GO-70 °C	4.5 ± 0.4	10 ppm	5.8
RhNP/GO-90 °C	5.2 ± 0.5	10 ppm	5.32

[a] Reaction conditions: 4-NP (1 equiv.), $NaBH_4$ (81 equiv.). [b] Core size (TEM). [c] RhNPs catalysts per 4-NP. [d] Rate constant.

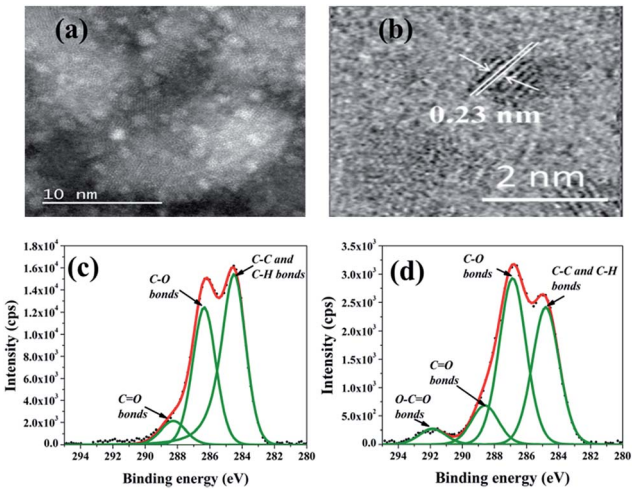

Fig. 1 (a) STEM image and (b) HRTEM of the RhNPs/GO-45 °C nanocatalyst. XPS spectra of C 1s on (c) GO and (d) RhNPs/GO-45 °C nanocatalyst.

stabilizing ligands with the lone pairs of the oxygen atoms in the formation of RhNPs.[36–38] The B. E. values at 307.6 and 312.8 eV are assigned to Rh $3d_{5/2}$ and Rh $3d_{3/2}$ of Rh(0) respectively,[39] indicating the presence of metallic Rh (Fig. S10†). A *ca.* 1 eV red shift of XPS peak of these very small RhNPs is observed and compared to bulk Rh, which is typical for very small metal NPs on a variety of support materials and is generally attributed to the reduced core-hole screening in metal clusters.[32] Such a size-dependent alteration of electronic structures[32] is seemingly concomitant with the enhanced catalytic properties (*vide infra*).

These results indicate that the high density of oxygen atom-containing functional groups on the GO surface interact with Rh atoms and therefore provide stabilization of RhNPs. A similar synthesis conducted under dark and only stirring in order to exclude the influence of light and power caused by the sonication showed no difference in the Rh^{3+} reduction to Rh(0) by GO. This confirms that the redox reaction between GO and Rh^{3+} accounts for the synthesis of RhNP/GO, as for the reaction proposed by Dai *et al.*[30] On the other hand, a galvanic reaction-like process in which reduction of Rh^{3+} to Rh nuclei occurs by electron transfer from GO may also be involved in the growth of the RhNPs after nucleation, accompanying GO oxidation.[31,32,40] This is also confirmed by XPS showing the increase of carboxylic groups of GO upon reduction of Rh^{3+} (Fig. 1d). The Raman spectra of the nanocatalyst RhNP/GO-45 °C showed no obvious change in the intensity ratio of I_D/I_G compared to pure GO, however (Fig. S11†), suggesting that the formation of RhNPs does not greatly reduce the size of the in-plane sp^2 domains of graphene.[30] Indeed, the XPS data suggest that the atomic content of Rh is only 1.9%, which is too low to cause a large structural damage to GO sheets.

3.2. 4-NP reduction by RhNP/GO nanocatalysts

The catalysis of reduction by $NaBH_4$ of the pollutant 4-nitrophenol (4-NP) in water (eqn (1)) to the useful dye 4-aminophenol was first probed; this is a trusted test reaction to further explore

the catalytic efficiency of NP surfaces and optimize catalytic conditions.[41–43]

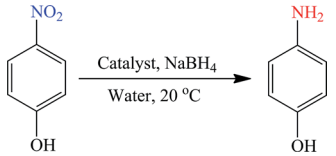

(1)

According to the reaction mechanism (see mechanistic details in the ESI†), the activation and dynamic restructuring of the NP surface are required, which eventually proceeds with an induction time if NP ligands are present.[44–46] Therefore, in the absence of surface restructuration if no ligand replacement is required, the 4-NP reduction catalyzed by surface-clean RhNP/GO would proceed with higher efficiency without induction time. The first attempt using 0.05 mol% catalyst in all the cases indicated that reduction was fast (in 40 s, the time for a complete scan) (ESI†), while control experiment showed the lack of any reactant conversion in the presence of only GO. Further decreasing the catalyst amount to 10 ppm (RhNPs per 4-NP) allows to easily monitor the reaction processes by UV-vis. spectroscopy, showing very fast 4-NP reduction without induction time (Table 1 and ESI Section 3†).

The catalytic efficiencies were shown to undergo a volcano-type relationship with respect to RhNP/GO nanocatalysts synthesized at various temperatures. The catalyst RhNP/GO-45 °C showed the highest reaction rate, $k_{app} = 11.8 \times 10^{-3}$ s^{-1}, 1.65 times higher than that of RhNP/GO-0 °C. The comparisons shown in Table S1† indicate that this catalyst showed the best efficiency ever obtained among various reported efficient catalysts. Remarkably, upon decreasing the total amount of RhNP/GO-45 °C to 1 ppm (RhNPs per 4-NP), high efficiency still remained, with $k_{app} = 4.29 \times 10^{-3}$ s^{-1} that is 1.4 times higher than the reaction rate obtained with 1 ppm of the catalyst RhNP/GO-0 °C under identical conditions. The remarkable efficiencies with exceptional low (ppm) amount of catalyst have so far never been reported and could be attributed to the ultrafine RhNP size and the very active surface-clean RhNPs. The presence of GO also increased the concentration of substrates near the surface Rh atoms,[47–49] benefiting to the catalytic efficiency.

3.3. Hydrolysis of ammonia–borane (AB) for H_2 generation

With the efficient RhNP/GO-45 °C nanocatalyst in hand, we then turned to another valuable reaction: the hydrolysis of ammonia–borane (AB) for H_2 generation. Owing to its high hydrogen content (19.6 wt%), high stability in the solid state and solution under ambient conditions, nontoxicity, and high solubility, AB has been considered as one of the leading contender in promising chemical H_2-storage materials.[50–59] Although many catalysts have been designed for the hydrolysis of AB, high-performance noble metal NPs still remain the most active catalysts for this reaction.[60–65] High catalyst loading of noble-metal catalyst and specific treatments are essential for the practical efficiency and sustainability, however. Herein we scrutinize the use of RhNP/GO-45 °C as a nanocatalyst for the hydrolysis of AB in water under air. This provides one of the highest turnover frequencies (TOFs) for H_2 generation near or at ambient temperature with low catalyst amounts.

The reaction profile in the presence of various amounts of RhNP/GO-45 °C is shown in Fig. S21.† The nearly stoichiometric amounts of hydrogen release (3 equiv. H_2 per AB), indicate that hydrolysis of AB catalyzed by RhNP/GO-45 °C proceeds according to eqn (2):

$$nH_3NBH_3 + 2nH_2O \xrightarrow[H_2O,r.t.,Air]{Rh/GO\text{-}45\,^\circ C} nNH_4^+ + nBO_2^- + 3nH_2 \quad (2)$$

At the beginning of the reaction, the decay of AB producing H_2 was fast and linear as a function of the reaction time. Later on, it became slower especially under lower catalyst amounts. The hydrolysis of AB at rt (25 ± 0.5 °C) was completed within the shortest time (7.75 min) when the amount of RhNP/GO-45 °C was 0.15 mol%, providing a turnover frequency (TOF) of 258 mol_{H_2} mol_{cat}^{-1} min^{-1}. The highest TOF was obtained with the optimum catalytic performance in the presence of 0.1 mol% catalyst for 9.5 min (TOF = 316 mol_{H_2} mol $_{cat}^{-1}$ min^{-1}), while a further decrease of catalyst amount led to a longer reaction time and therefore the decrease of TOF values (Table S2†). On the other hand, the uncatalyzed thermal reaction in the absence of catalyst showed negligible dehydrogenation of AB at the early stage of the reaction. The catalytic efficiencies obtained herein are comparable to the best previously reported performances achieved using several noble metal-based NP catalysts, showing the high efficiency of the present RhNP/GO system for hydrolysis of AB (Table S3†).

3.4. Hydrolysis mechanism

Fig. 2a demonstrates that the logarithmic plot of the calculated initial reaction rate *vs.* catalyst concentration has a slope of

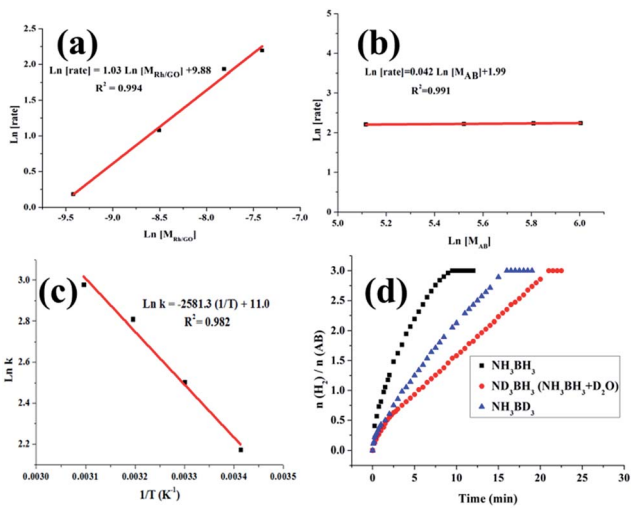

Fig. 2 (a) The plot of hydrogen generation rate *vs.* the concentration of RhNPs/GO-45 °C both in natural logarithmic scale. (b) The plot of hydrogen generation rate *vs.* the concentration of AB both in natural logarithmic scale. (c) Arrhenius plots obtained from the kinetic data. (d) Hydrogen evolution from NH_3BH_3, ND_3BH_3, and NH_3BD_3 catalyzed by 0.1 mol% RhNP/GO-45 °C.

 This journal is © The Royal Society of Chemistry 2017

1.03, indicating that the hydrolysis of AB catalyzed by RhNP/GO-45 °C follows a first-order kinetics with respect to catalyst concentration. The nearly horizontal line (slope of 0.042) indicates that the hydrolysis of AB catalyzed by RhNP/GO-45 °C is zero-order with respect to the AB concentration (Fig. 2b). This implies that AB activation is easy and thus rules out the possibility that the activation of AB in the rate-determining step (RDS). Furthermore, the activation energy (E_a) of hydrolysis of AB was determined to be approximately 21.4 kJ mol^{-1} (Fig. 2c and calculations), one of the lowest E_a values compared to the literature (Table S3†).

Although the catalytic rates in the hydrolysis of AB catalyzed by RhNP/GO-45 °C is independent of the AB concentration, the kinetic isotope effects (KIEs)[66–68] were further investigated to shed light on the RDS of the reaction. Specifically in the hydrolysis of AB, the KIE value should tell if N–H or B–H or both bonds are broken or not during the RDS.[69–73]

The hydrolysis of the deuterated products of AB (see their synthesis in the ESI†) in the presence of RhNP/GO-45 °C results in slower reaction rates (Fig. 2d). A KIE of 1.33 was determined for deuteration at the boron site (NH_3BD_3), which indicates a similar dehydrogenation behavior to that of AB in H_2O. This shows the absence of large KIE for hydrolysis of AB deuterated at the boron site (NH_3BD_3). A larger KIE (2.57) was found for ND_3BH_3, suggesting that the O–H bond cleavage of H_2O might be in the RDS. This would be similar to the metal-catalyzed borohydride hydrolysis, in which half of the hydrogen comes from water.[74] Indeed, H_2O is activated by oxidative addition of a O–H bond on noble metal NP surfaces, forming adsorbed –OH and –H species. For instance, well-known precedents are found in the role of PtNPs as redox catalysts in water photo-splitting.[75,76] On the other hand, since the reaction rate is zero-order with respect to concentration of AB, H_2O dissociation alone as the RDS is not possible. Moreover, considering that the energy for the cleavage of the O–H bond in water (~493 kJ mol^{-1})[77] is higher than those of B–N and B–H bond (~117 and ~430 kJ mol^{-1}, respectively),[78] and the low energy barrier (E_a) obtained in the present hydrolysis reaction, the involvement of H_2O activation in the RDS of the hydrolysis is energetically favorable. Thus H_2O is most likely activated by an indirect O–H bond cleavage to form –H and –OH species promoted by AB in the presence of RhNP/GO-45 °C.[72,73] Activation proceeds similarly in H_2O activation for $NaBH_4$ hydrolysis. We also suggest that the "hydridic" B–H hydrogen atom of AB forms a hydrogen bond with an "acidic" hydrogen atom of water in the ground state and that this B–Hδ^-···Hδ^+–O system undergoes oxidative addition followed by H_2 elimination on the Rh surface. Based on this understanding and experimental results, the hydrolysis of AB catalyzed by RhNPs/GO-45 °C in water is best presented overall as shown in Fig. 3.

The B–N bond in the AB is dissociated, since the NH_3 group does not participate in the hydrolysis.[60] On the other hand, the presence of GO facilitates the adsorption of the reactant or desorption of products in water,[47–49] thus accelerating the overall process and improving the catalytic activity.

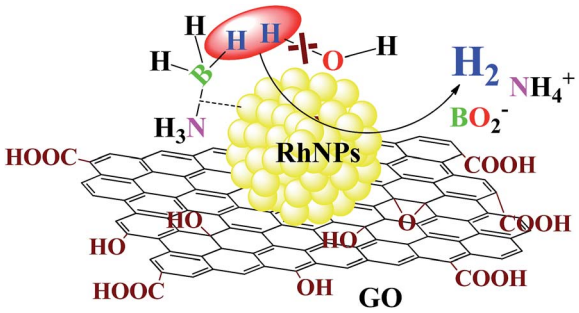

Fig. 3 Proposed mechanism for the hydrolysis of AB by catalyzed by RhNP/GO-45 °C.

3.5. Extension to the synthesis of other high efficient AuNPs/GO, PdNPs/GO, CuNPs/GO, and CuPd NPs/GO nanocatalysts

The general principle of transition-metal–GO nanocatalysts is extended to the synthesis of AuNPs/GO, PdNPs/GO, CuNPs/GO, and CuPd NPs/GO at 45 °C under identical conditions. In the case of AuNPs/GO, reduction of Au^{3+} by GO ($Au^{3+}/Au^0 = 1.5$ V *vs.* SHE) results in the high efficient AuNPs/GO nanocatalyst with AuNPs of 3.3 nm (Fig. S27†), as exemplified by the 0.05 mol% AuNPs/GO nanocatalyst catalyzed 4-NP reduction in water (Fig. S28†) without induction time and remarkable efficiency ($k_{app} = 3.7 \times 10^{-3}$ s^{-1}) compared to the recently reported values (Table S2†).

Another challenging example is the synthesis of first raw metal NPs by reduction the metal precursors with GO, because the redox potential of $M^{2+/3+}/M(0)$ compared to the oxidation potential of GO makes the reaction endergonic. Upon heating at 45 °C, however, Cu^{2+} reduction ($Cu^{2+}/Cu^0 = 0.34$ V *vs.* SHE) by GO proceeds due to the fast follow-up Cu atom aggregation that shifts the apparently unfavorable redox process. Thus the formation of CuNPs/GO in this way was confirmed by both UV-vis. spectroscopy and XPS. No SPB was observed due to the small CuNP size (3.0 nm), but the surface Cu(0) oxidation state is shown by XPS (Fig. S30†). On the other hand, 4-NP reduction is successfully achieved using 0.5% mol CuNPs/GO catalyst with no induction time and a high efficiency of 5.2×10^{-3} s^{-1} (k_{app}). The absence of induction time in the 4-NP reduction suggests that activation and dynamic restructuring of the Cu(0) surface is not necessary due to the absence of molecular ligand. Note that even weakly stabilizing triazole-based ligand on CuNPs provoke the requirement of an induction time for 4-NP reduction.[79] The high efficiency of the CuNPs/GO nanocatalyst was also confirmed by the "click" reaction[80–83] between benzyl azide and phenylacetylene (details see ESI†), in which 93% isolated yield was achieved at 35 °C for 24 h using only 0.01 mol% of CuNPs (eqn (3)); this is one of the lowest catalyst amounts among recent literature values.

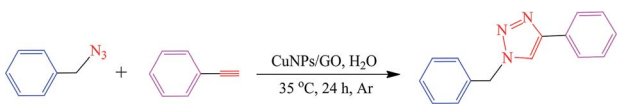

(3)

XPS suggests that the active Cu^{I} species is formed in the native oxide layer on the Cu surface through comproportionation of Cu^{0} and Cu^{II} (Fig. S30†).

Pd/Cu nanocatalysts have been successfully applied to Sonogashira coupling reactions, in which two cooperative catalytic cycles of Pd and Cu form the mechanism; thus an increased efficiency of Sonogashira coupling reaction is expected.[84,85] We assumed that the double reduction of equimolar amount of Pd^{2+} ($Pd^{2+}/Pd^{0} = 1.5$ V *vs.* SHE) and Cu^{2+} by GO could result in a valuable heterogeneous catalyst for Sonogashira coupling reaction under hopefully very favorable conditions. Thus CuPd NPs/GO nanocatalyst prepared in this way was characterized by TEM and XPS. TEM showed the NP size is around 3.5 nm (Fig. S34†), while XPS suggested the molar ratio is Pd : Cu = 1 : 1.35. Moreover, the CuPd NPs surface showed both the surface Cu(0) and the Cu^{2+} oxidation states of Cu (Fig. S35†), and the XPS peak $3d_{5/2}$ of Pd(0) located at 335.9 eV (Fig. S36† and discussions). For comparison, CuNPs/GO and PdNPs/GO nanocatalysts were separately prepared and tested in the Sonogashira coupling between iodobenzene and phenylacetylene in water at room temperature (rt) for 24 h with 0.05 mol% metal loading. PdNPs/GO nanocatalyst with Pd size of 2.8 nm showed an acceptable 85% conversion, while in the case of Cu NPs/GO nanocatalyst the conversion was less than 20%. Note that the result of PdNP/GO is already very good at rt, but with combined Cu and Pd, remarkably conversion was quantitative with 93% isolated yield in this Sonogashira coupling reaction (eqn (4)). Therefore, synergistic CuPd NPs/GO nanocatalyst is an excellent catalyst for Sonogashira coupling in water at rt, *i.e.* under environmentally-friendly condition.

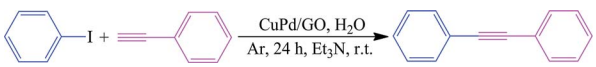

(4)

Finally, the reusability of the catalyst was studied using RhNP/GO-45 °C nanocatalyst in the hydrolysis of AB in water by continuous addition of a new proportion of AB aqueous solution when the previous run was completed. In this way RhNP/GO-45 °C was successfully recycled four times (Fig. 4). Therefore it is an excellent catalyst for the hydrolysis reaction. The observed little decrease of activity in the fourth run is probably ascribed to the aggregation of RhNPs as shown by TEM image taken after recycling experiments (Fig. S39†). It is due to the slight deactivation effect of the hydrolysis product metaborate[56,60,61,86] that accumulates during the hydrolysis and partly inhibits the catalytically active Rh surface atoms, and to the dilution of the reactant in water.

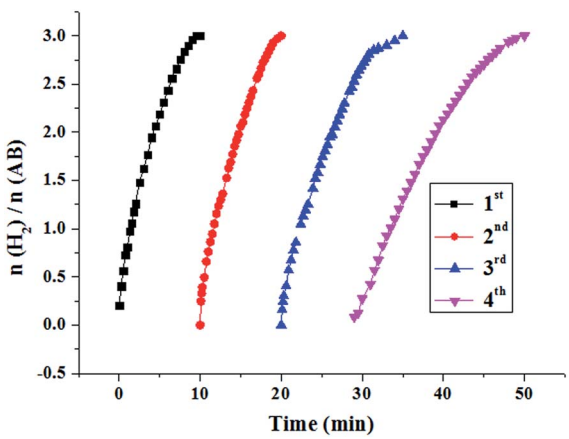

Fig. 4 Time plots of the catalytic dehydrogenation of AB by the nanocatalyst RhNPs/GO-45 °C for the reusability test.

4. Conclusions

In summary, a simple, clean redox reaction between various transition metal cations and GO has been shown here to lead to the synthesis of ultrafine, surface-clean metal NPs on graphene oxide with good monodispersity. This method avoids the formation of reactant residues inhibiting the catalytic NP surface. The appropriate choice of temperature during the synthesis improves the reduction efficiency and enhances the interaction between the RhNPs and GO. Consequently, the nanocatalyst RhNP/GO without any other ligand shows exceptional efficiency in the 4-NP reduction down to 1 ppm metal level, and it is also very efficient for the hydrolysis of AB to produce H_2. The KIE studies allow the clarification of the RDS for AB hydrolysis. Moreover, this strategy also produces other excellent metal NP/GO catalysts for redox reactions in general, showing high efficiency in 4-NP reduction, Sonogashira coupling at rt, click reaction and hydrolysis of AB for hydrogen production with low amounts of catalytic metals. The activation of NP/GO by GO as ligand recalls the efficient catalysis using oxides as ligands,[87] although the NP–GO interactions are of different nature here, of rather synergetic supramolecular type. The principles and clean and simple catalytic method presented herein may be extended to other transition-metal nanocatalysts and should contribute to the rational design of efficient nanocatalysts for a large variety of chemical reactions.

Conflicts of interest

There are no conflicts to declare.

Acknowledgements

Financial support from the China Scholarship Council (CSC) of the People's Republic of China (grant to C. W.), the Universities of Bordeaux, Toulouse 3, Basque Country and San Sebastian, the LCC (Toulouse), the CNRS and the FP7-People-Irses-Higraphen Project No. 612704 is gratefully acknowledged.

Notes and references

1 A. Fihri, M. Bouhrara, B. Nekoueihahraki, J. M. Basset and V. Polhettiwar, *Chem. Soc. Rev.*, 2011, **40**, 5181–5203.
2 L. M. Bronstein and Z. B. Shifrina, *Chem. Rev.*, 2011, **111**, 5301–5344.
3 A. Balanta, C. Godart and C. Claver, *Chem. Soc. Rev.*, 2011, **40**, 4973–4985.

 This journal is © The Royal Society of Chemistry 2017

4 E. Gross, J. H.-C. Liu, F. D. Toste and G. A. Somorjai, *Nat. Chem.*, 2012, **4**, 947–952.
5 J. D. Scholden, B. C. Leal and J. Dupont, *ACS Catal.*, 2012, **2**, 184–200.
6 M. Sankar, N. Dimitratos, P. J. Miedjack, P. P. Wells, C. J. Kiely and G. J. Hutchings, *Chem. Soc. Rev.*, 2012, **41**, 8099–8139.
7 D. Astruc, *Nat. Chem.*, 2012, **4**, 255–267.
8 M. Haruta, *Angew. Chem., Int. Ed.*, 2014, **53**, 52–56.
9 M. B. Gawande, A. Goswami, F.-X. Felpin, T. Asefa, X. X. Huang, R. Silva, X. X. Zou, R. Zboril and R. S. Varma, *Chem. Rev.*, 2016, **116**, 3722.
10 C. Amiens, D. Ciuculescu-Pradines and K. Philippot, *Coord. Chem. Rev.*, 2016, **308**, 409–432.
11 Y. Xia, K. D. Gilroy, H.-C. Peng and X. Xia, *Angew. Chem., Int. Ed.*, 2017, **56**, 60–95.
12 D. Wang and D. Astruc, *Chem. Soc. Rev.*, 2017, **46**, 816–854.
13 P. Liu, R. Qin, G. Fu and N. Zheng, *J. Am. Chem. Soc.*, 2017, **139**, 2122–2131.
14 N. Toshima and T. Yomezawa, *New J. Chem.*, 1998, **22**, 1179–1201.
15 D. Astruc, F. Lu and J. Ruiz, *Angew. Chem., Int. Ed.*, 2005, **44**, 7852–7872.
16 N. T. S. Phan, M. Van Der Sluys and C. W. Jones, *Adv. Synth. Catal.*, 2006, **348**, 609–679.
17 V. S. Myers, M. G. Weir, E. V. Carino, D. F. Yancey, S. Pande and R. M. Crooks, *Chem. Sci.*, 2011, **2**, 1632–1646.
18 J. A. Lopez-Sanchez, N. Dimitratos, C. Hammond, G. L. Brett, L. Kesavan, S. White, P. Miedziak, R. Tiruvalam, R. L. Jenkins, A. F. Carley, D. Knight, C. J. Kiely and G. J. Hutchings, *Nat. Chem.*, 2011, **3**, 551–556.
19 C. H. Cui, L. Gan, M. Heggen, S. Rudi and P. Strasser, *Nat. Mater.*, 2013, **12**, 765–771.
20 G. Prieto, J. Zecevic, H. Friederich, K. P. de Jong and P. E. De Jongh, *Nat. Mater.*, 2013, **12**, 34–39.
21 Z. Niu and Y. Li, *Chem. Mater.*, 2014, **26**, 72–83.
22 K. Na, M. Choi, O. M. Yaghi and G. A. Somorjai, *Nano Lett.*, 2014, **14**, 5979–5983.
23 R. R. Haikal, A. M. Elmansi, A. B. Soliman, P. Aly, Y. S. Hassan, M. R. Berber, I. H. Hafez, A. Hassanien and M. H. Alkordi, *RSC Adv.*, 2016, **6**, 94547–94555.
24 S. Navalon, A. Dhakshinamoorthy, M. Alvaro and H. Garcia, *Chem. Rev.*, 2014, **114**(43), 5288–5301.
25 D. R. Dreyer, A. D. Todd and C. W. Bielawski, *Chem. Soc. Rev.*, 2014, **114**, 6179–6212.
26 X. B. Fan, G. L. Zhang and F. B. Zhang, *Chem. Soc. Rev.*, 2015, **44**, 3023–3035.
27 N. M. Julkapli and S. Bagheri, *Int. J. Hydrogen Energy*, 2015, **40**, 948–979.
28 S. Navalon, A. Dhakshinamoorthy, M. Alvaro and H. Garcia, *Coord. Chem. Rev.*, 2016, **312**, 99–148.
29 C. Han, N. Zhang and Y. J. Xu, *Nano Today*, 2016, **11**, 351–372.
30 H. C. Choi, M. Shim, S. Bangsaruntip and H. Dai, *J. Am. Chem. Soc.*, 2002, **124**, 9058–9059.
31 X. Chen, G. Wu, J. Chen, X. Chen, Z. Xie and X. Wang, *J. Am. Chem. Soc.*, 2011, **133**, 3693–3695.
32 H. Yin, H. Tang, D. Wang, Y. Gao and Z. Tang, *ACS Nano*, 2012, **6**, 8288–8297.
33 Y. Bia and G. Lu, *Chem. Commun.*, 2008, 6402–6404.
34 J. G. Radich and P. V. Kamat, *ACS Nano*, 2013, **7**, 5546–5557.
35 F. Durap, M. Zahmakıran and S. Özkar, *Appl. Catal., A*, 2009, **369**, 53–59.
36 P. R. Kannan, A. Swami, D. Srisathiyanarayanan, P. S. Shirude, R. Pasricha, A. B. Mandale and M. Sastry, *Langmuir*, 2004, **20**, 7825–7836.
37 R. Pasricha, S. Gupta and A. K. Srivastava, *Small*, 2009, **5**, 2253–2259.
38 F. Li, Y. Guo, Y. Liu, J. Yan, W. Wang and J. Gao, *Carbon*, 2014, **67**, 617–626.
39 D. Özhava and S. Özkar, *Appl. Catal., B*, 2016, **181**, 716–726.
40 Y. Qin, J. Li, Y. Kong, X. Li, Y. Tao, S. Li and Y. Wang, *Nanoscale*, 2014, **6**, 1281–1285.
41 N. Pradhan, A. Pal and T. Pal, *Colloids Surf., A*, 2002, **196**, 247–257.
42 T. Aditya, A. Pal and T. Pal, *Chem. Commun.*, 2015, **51**, 9410–9431.
43 P. Zhao, X. Feng, D. Huang, G. Yang and D. Astruc, *Coord. Chem. Rev.*, 2015, **287**, 114–136.
44 S. Wunder, Y. Lu, M. Albrecht and M. Ballauff, *ACS Catal.*, 2011, **1**, 908–916.
45 S. Gu, Y. Lu, J. Kaiser, M. Albrecht and M. Ballauff, *Phys. Chem. Chem. Phys.*, 2015, **17**, 28137–28143.
46 Y. Lu and M. Ballauff, *Prog. Polym. Sci.*, 2016, **59**, 86–104.
47 T. Wu, L. Zhang, J. Gao, Y. Liu, C. Gao and J. Yan, *J. Mater. Chem. A*, 2013, **1**, 7384–7390.
48 J.-J. Lv, A.-J. Wang, X. Ma, R.-Y. Xiang, J.-R. Chen and J.-J. Feng, *J. Mater. Chem. A*, 2015, **3**, 290–296.
49 P. Song, L.-L. He, A.-J. Wang, L.-P. Mei, S.-X. Zhong, J.-R. Chen and J.-J. Feng, *J. Mater. Chem. A*, 2015, **3**, 5321–5327.
50 Q. Xu and M. Chandra, *J. Power Sources*, 2006, **163**, 364–370.
51 M. Chandra and Q. Xu, *J. Power Sources*, 2007, **168**, 135–142.
52 F. H. Stephens, V. Pons and R. T. Baker, *Dalton Trans.*, 2007, 2613–2626.
53 J.-M. Yan, X.-B. Zhang, S. Han, H. Shioyama and Q. Xu, *Angew. Chem., Int. Ed.*, 2008, **47**, 2287–2289.
54 C. W. Hamilton, R. T. Baker, A. Staubitz and I. Manners, *Chem. Soc. Rev.*, 2009, **38**, 279–293.
55 H.-L. Jiang, S. K. Singh, J.-M. Yan, X.-B. Zhang and Q. Xu, *ChemSusChem*, 2010, **3**, 541–549.
56 O. Metin, V. Mazumder, S. Özkar and S. S. Sun, *J. Am. Chem. Soc.*, 2010, **132**, 1468–1469.
57 A. Staubitz, A. P. M. Robertson and I. Manners, *Chem. Rev.*, 2010, **110**, 4079–4124.
58 Q. L. Zhu and Q. Xu, *Energy Environ. Sci.*, 2015, **8**, 478–512.
59 Q.-L. Zhu and Q. Xu, *Chem*, 2016, **1**, 220–245.
60 Q.-L. Zhu, J. Li and Q. Xu, *J. Am. Chem. Soc.*, 2013, **135**, 10210–10213.
61 M. Rakap, *Appl. Catal., B*, 2015, **163**, 129–134.
62 W.-W. Zhan, Q.-L. Zhu and Q. Xu, *ACS Catal.*, 2016, **6**, 6892–6905.
63 M. A. Khalily, H. Eren, S. Akbayrak, H. H. Susapto, N. Biyikli, S. Özkar and M. O. Guler, *Angew. Chem., Int. Ed.*, 2016, **55**, 12257–12261.

This journal is © The Royal Society of Chemistry 2017

64 S. Akbayrak, Y. Tonbul and S. Özkar, *Appl. Catal., B*, 2016, **198**, 162–170.
65 K. Mori, K. Miyawaki and H. Yamashita, *ACS Catal.*, 2016, **6**, 3128–3135.
66 K. C. Westaway, *J. Labelled Compd. Radiopharm.*, 2007, **50**, 989–1005.
67 G. Guella, B. Patton and A. Miotello, *J. Phys. Chem. C*, 2007, **111**, 18744–18750.
68 E. M. Simmons and J. F. Hartwig, *Angew. Chem., Int. Ed.*, 2012, **51**, 3066–3072.
69 R. J. Keaton, J. M. Blacquiere and R. T. Baker, *J. Am. Chem. Soc.*, 2007, **129**, 1844–1845.
70 P. Bhattacharya, J. A. Krause and H. Guan, *J. Am. Chem. Soc.*, 2014, **136**, 11153–11161.
71 J. A. Buss, G. A. Edouard, C. Cheng, J. Shi and T. Agapie, *J. Am. Chem. Soc.*, 2014, **136**, 11272–11275.
72 W. Chen, D. Li, Z. Wang, G. Qian, Z. Sui, X. Duan, X. Zhou, I. Yeboah and D. Chen, *AIChE J.*, 2017, **63**, 60–65.
73 Z. Li, T. He, L. Liu, W. Chen, M. Zhang, G. Wu and P. Chen, *Chem. Sci.*, 2017, **8**, 781–788.
74 B. H. Liu and Z. P. Li, *J. Power Sources*, 2009, **187**, 527–534.
75 J.-M. Lehn and J.-P. Sauvage, *Nouv. J. Chim.*, 1977, **1**, 449–451.
76 A. Hagfeldt and M. Grätzel, *Chem. Rev.*, 1995, **95**, 49–68.
77 P. R. Rablen, *J. Am. Chem. Soc.*, 1997, **119**, 8350–8360.
78 L. R. Peebles and P. Marshall, *J. Chem. Phys.*, 2002, **117**, 3132–3138.
79 C. Wang, R. Ciganda, L. Salmon, D. Gregurec, J. Irigoyen, S. Moya, J. Ruiz and D. Astruc, *Angew. Chem., Int. Ed.*, 2016, **55**, 3091–3095.
80 M. Meldal and C. W. Tornøe, *Chem. Rev.*, 2008, **108**, 2952–3015.
81 J. E. Hein and V. V. Fokin, *Chem. Soc. Rev.*, 2010, **39**, 1302–1315.
82 F. Alonso, Y. Moglie and G. Radivoy, *Acc. Chem. Res.*, 2015, **48**, 2516–2528.
83 C. Wang, D. Ikhlef, S. Kahlal, J. Y. Saillard and D. Astruc, *Coord. Chem. Rev.*, 2016, **316**, 1–20.
84 R. Chinchilla and C. Nájera, *Chem. Rev.*, 2007, **107**, 874–922.
85 R. Chinchilla and C. Nájera, *Chem. Soc. Rev.*, 2011, **40**, 5084–5121.
86 W. Chen, J. Ji, X. Feng, X. Duan, G. Qian, P. Li, X. Zhou, D. Chen and W. Yuan, *J. Am. Chem. Soc.*, 2014, **136**, 16736–16739.
87 D. A. Pelletier and J.-M. Basset, *Acc. Chem. Res.*, 2016, **49**, 664–677.

This journal is © The Royal Society of Chemistry 2017